J Mater Sci (2011) 46:1705–1713
DOI 10.1007/s10853-010-4988-0

Applicability of empirical models for evaluation of stress ratio effect on the durability of fiber-reinforced creep rupture–susceptible composites

J. Andersons · Yu. Paramonov

Received: 1 June 2010 / Accepted: 6 October 2010 / Published online: 21 October 2010

Abstract Fiber-reinforced polymer–matrix composites are known to exhibit loading rate- and time-dependent mechanical response. Their fatigue strength is determined by a complex interaction of damage processes governed by loading duration and cycle number. Apart from mechanistic approaches, a number of empirical models of various sophistication have been proposed to predict the durability of composites, differing in the amount of experimental data needed for their application. The accuracy of several such models is evaluated by comparing the prediction to the experimentally determined stress ratio effect on fatigue life of glass fiber-reinforced polyester–matrix composite. It is found that the accuracy of prediction generally improves with increasing the amount of test data needed for model calibration. However, the most accurate method of fatigue life estimation, among the selected ones, is by the modified Goodman diagram.

Introduction

Fiber-reinforced polymer–matrix composites are known to exhibit loading rate- and time-dependent mechanical response due to viscoelastoplasticity of the matrix and time-dependent response of some types of fibers (e.g., glass, aramid, natural fibers), see e.g. [1, 2]. Therefore, the durability of such composites under cyclic loading is governed by a combination of damage processes due to loading time and due to the number of load recursions. The damage suffered by fiber-reinforced composites includes fiber breaks, debonding, delamination, and matrix cracking, that develop and interact during loading [3] leading to ultimate failure of the material. Along with mechanistic models of fatigue, a number of simple empirical relations for fatigue life prediction have been proposed.

Constant life diagrams seek to represent the stress amplitude, leading to fracture at a given number of load cycles, as a function of the mean stress under constant-amplitude cyclic loading. A number of such relations have been proposed for composite materials, providing reasonably good approximation of test results at different stress ratios [4–8]. Another group of models relate durability to the level of damage accumulated during fatigue loading, characterized by the reduction of the modulus of elasticity or residual strength [9–11]. Each of the empirical models mentioned has been applied to test results of several composites under different loading conditions that should usually allow evaluation of the applicability range and expected accuracy of the model.

An alternative approach is chosen in this study, namely, several models, differing in the amount of experimental information needed for model calibration, are compared against fatigue life data set of a glass fiber-reinforced polyester–matrix composite of relatively complex lay-up, selected for application in wind turbine blades. Such a comparison allows weighing the gain in the accuracy of model prediction against the need for more extensive test program necessary for calibration of the relatively sophisticated models. The trade-off in prediction accuracy versus the amount of calibration testing for different models then can be used as an additional selection criterion, complimenting the

J. Andersons (✉)
Institute of Polymer Mechanics, University of Latvia,
Aizkraukles 23, Riga, LV 1006, Latvia
e-mail: janis.andersons@pmi.lv

Yu. Paramonov
Aviation Institute, Riga Technical University, Lomonosova 1,
Riga, LV 1019, Latvia

traditional approach of seeking a single best empirical model.

Prediction of the durability of a glass/polyester composite under uniaxial cyclic loading is considered. Tension–tension cycling in the predominant UD reinforcement direction is studied, with stress ratios in the rage from 0.1 to 1. The results are expected to be applicable for fiber-dominated glass fiber-reinforced thermoset polymer–matrix composites susceptible to creep rupture. Moreover, as the empirical models of fatigue under spectrum [11, 12] and multiaxial [13] loading usually incorporate fatigue strengths in uniaxial constant-amplitude loading, the findings should be relevant also for prediction of durability under more complicated fatigue loading scenarios.

The paper is organized as follows: first, a brief description of the material and tests is given. Then several models are selected, concisely presented in the order of increasing complexity, and applied to predict the effect of stress ratio on fatigue life. Finally, the results obtained are analyzed in terms of accuracy of the models and ease of their implementation.

Experimental

The experimental data used in fatigue modeling have been reported previously [14–17] in a different context. For convenience and completeness, we concisely recapitulate material and test description below.

The composite material tested was produced by hand lay-up, and comprised chopped strand mat (CSM), unidirectionally reinforced (UD), and fabric layers in the following sequence: $[\text{CSM/fabric/(CSM, UD)}_2]_S$. The resin used was an orthophthalic polyester Norpol 410M910. The fiber volume fraction amounted to 41%. Specimens of dog-bone shape were used for tensile static strength [15], creep rupture strength [17], residual strength [15, 16], and fatigue tests [14, 17]. The cyclic tests were run under stress control at ambient conditions. Durability was determined for stress ratios $R = 0.1$, 0.3, 0.5, 0.8, 0.9 and $R = 1$ (creep rupture strength). The respective S–N curves [17] are shown in Fig. 1 and creep rupture strength data presented in Fig. 2. The fatigue failure mechanism remained the same in the whole range of stress ratios and lifetimes as suggested by fracture surface morphology. This is also corroborated by the relative increase of the dynamic compliance during fatigue lifetime which, while exhibiting considerable scatter, did not depend on the stress ratio and amounted to [14] ca. 9%.

The fatigue loading frequencies used were 2, 4, and 17 Hz. Although no systematic statistical study on the frequency effect on fatigue life was performed, test data shown in Fig. 1 suggested that this effect, if any, was negligible for fatigue design purposes in the frequency range covered. For $R = 0.9$ the frequency of 4 Hz was used, while for the other stress ratios studied the apparent absence of a frequency effect allowed to use higher test frequency for low amplitude (and higher lifetime) tests. The test data were approximated by linear relations in semi-logarithmic co-ordinates as follows: $\log N = C - B\sigma_{\max}$ for fatigue data, $\log(t/t_0) = C - B\sigma$ for creep rupture strength (time to fracture t was expressed in seconds and $t_0 = 1$ s chosen). The parameters of regression lines are presented in Table 1.

Selection of empirical fatigue models

The vast range of the empirical fatigue models developed for stress ratio effect evaluation in composite materials [4–10] can be classified, apart from mechanistic considerations, also based on the amount of testing needed for model calibration. We compare models that use as their input the following experimental data:

(i) tensile strength,
(ii) one fatigue curve at a fixed stress ratio,
(iii) two such curves at different stress ratios,
(iv) two fatigue curves at different stress ratios and additional residual property measurements.

Glass fiber/polymer matrix composites are expected to be sensitive to the static component of fatigue load (see also Fig. 2 for time-dependence of tensile strength of the present material). Therefore, whenever possible, we select models from the above groups that explicitly account for contribution of time- and cycle-dependent fatigue, as detailed below.

A recently proposed model [18, 19] is unique in the field of composite fatigue studies in that it uses just static strength characteristics (average and standard deviation) to predict fatigue life at constant-amplitude cyclic loading.

Several models have been proposed that use one experimentally determined fatigue curve at a specific stress ratio to predict, usually via invoking an effective stress concept, fatigue strength at an arbitrary R. Most of the definitions of such effective stresses have their origins in metal fatigue. Therefore, their applicability to polymer composites is, at best, limited to particular materials and loading conditions as, for example, that of Smith–Watson–Topper parameter, see [20, 21]. By contrast, a strain energy range-based approach has been shown to accurately describe both the effect of stress ratio and of loading direction (with respect to principal material axes) under uniaxial fatigue [22–25].

The simplest of constant life diagrams are also based on one fatigue curve, in conjunction with static strengths [26]. However, the static strength can be treated as the limit for

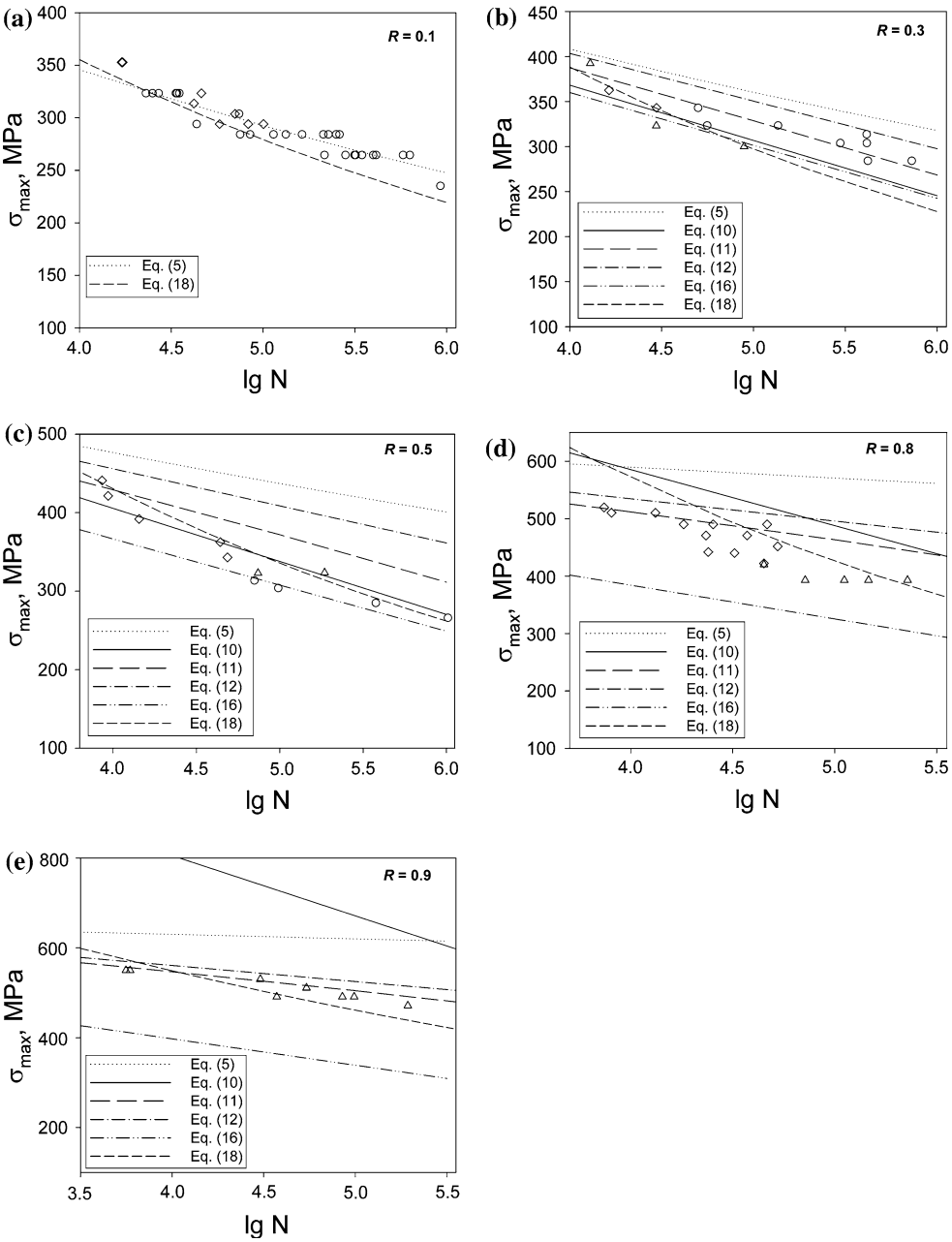

Fig. 1 *S–N* curves at stress ratio $R = 0.1$ (**a**), 0.3 (**b**), 0.5 (**c**), 0.8 (**d**), and 0.9 (**e**). The fatigue tests were performed at loading frequency $f = 17$ Hz (*circle*), 4 Hz (*triangle*), and 2 Hz (*diamond*)

fatigue strength at high stress ratios only for composites exhibiting little or no static fatigue. It has been repeatedly demonstrated, see e.g. [17, 27, 28], that for glass fiber-reinforced composites, the limit for fatigue strength at high mean cycle stresses is creep rupture strength at the loading time of interest. Therefore, in this study we select from the numerous constant life diagrams available [4–8] only those that incorporate the static strength dependence on time under load. This leaves the (appropriately modified) Goodman diagram [17, 27] and an interpolation of fatigue strength as a function of stress ratio [34, 35] that both need two fatigue curves for model calibration: experimental static fatigue data ($R = 1$) and a fatigue curve at another stress ratio.

Residual strength models require additional data, characterizing variation of the remaining strength during loading, for their calibration [9–11]. Only few of them, however, incorporate creep rupture phenomenon [2, 28, 29]. We choose to apply in the following the relatively simple yet sufficiently general and accurate model [2], needing fatigue curves at two stress ratios and residual strength data.

The lack of sufficiently detailed stiffness degradation data, needed for verification and calibration of the residual stiffness models, precluded their application to the composite material considered. However, records of compliance variation rate and limit values [14] enabled application of a

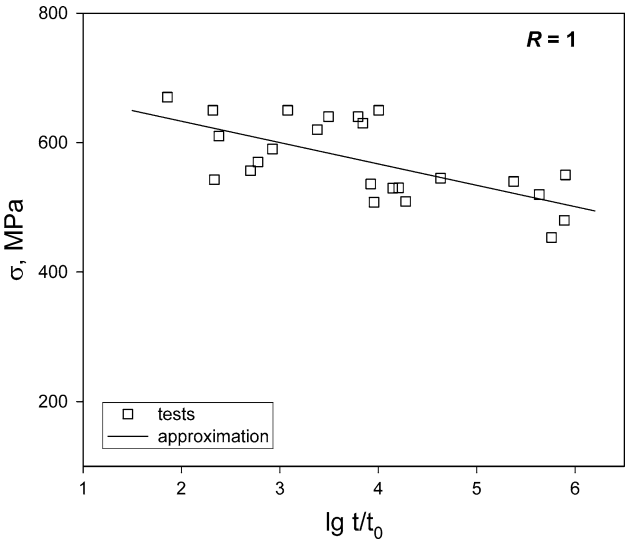

Fig. 2 Creep strength versus time under load in tension

Table 1 Parameters of *S–N* diagrams $\log N = C - B\sigma_{max}$ for fatigue and $\log (t/t_0) = C - B\sigma$ for creep strength

R	C	B (MPa^{-1})
0.1	10	0.017
0.3	10.8	0.018
0.5	8.6	0.011
0.8	9.1	0.01
0.9	13.6	0.018
1	11.2	0.013

damage monitoring-based durability evaluation technique [30].

Application of the selected models

Static strength–fatigue life relation

The most economical, in terms of testing program necessary for calibration, fatigue model relates the fatigue life under cyclic loading to the distribution of static strength [18, 19]. Treating subsequent load cycles as independent strength tests with the probability of failure in a single test given by p, the fatigue life N (defined as the number of load cycles maximizing the function P, where $P = np(1-p)^{n-1}$ is the probability of one and only one failure between 1 and n cycles) is obtained as

$$N = -\frac{1}{\ln(1-p)}. \tag{1}$$

For the loading case of interest here, $0 < R < 1$, the cumulative failure probability is further approximated by the two-parameter Weibull distribution

$$p = 1 - \exp\left[-\left(\frac{\sigma_{max}}{\beta}\right)^{\alpha}\right] \tag{2}$$

with the parameters related to the mean, σ_{st}, and the standard deviation, s, of the tensile strength as follows

$$1 - \frac{1}{\alpha} = \left(\frac{\sigma_{st}}{\beta}\right)^{\alpha} \tag{3}$$

$$\exp\left[-\left(\frac{x_1}{\beta}\right)^{\alpha}\right] - \exp\left[-\left(\frac{x_2}{\beta}\right)^{\alpha}\right] = 0.98$$

where

$$x_1 = \sigma_{st} - 2.326(1-R)s \tag{4}$$

$$x_2 = \sigma_{st} + 2.326s.$$

Combining Eqs. 1 and 2, one obtains for fatigue life at cyclic loading with maximum stress σ_{max}

$$N = \left(\frac{\sigma_{max}}{\beta}\right)^{-\alpha} \tag{5}$$

where the Weibull parameters α, β, determined by Eqs. 3 and 4, depend only on the static strength characteristics and the stress ratio of the cyclic loading.

Based on tension tests [15], $\sigma_{st} = 672$ MPa and $s = 21$ MPa. However, the fatigue diagrams predicted according to Eq. 5 using these strength characteristics disagree markedly with the fatigue test results (e.g., fatigue strength for $R = 0.1$ is overpredicted by a factor of 1.5–1.9 within the experimental durability range). It should be noted that the results are rather sensitive to the value of s [18], which was evaluated here from only 14 tension tests [15].

As an alternative, s was treated as a fitting parameter and its value determined so that Eq. 5 matched the fatigue test data at $R = 0.1$. The value of $s = 78$ MPa (together with the previous, experimental estimate of σ_{st}) provided a good approximation of the fatigue data as seen in Fig. 1a. The same best-fit estimate of s was further applied to predict the *S–N* diagrams at the other stress ratios considered. It is seen in Fig. 1b–e that the theoretical diagrams given by Eq. 5 systematically deviate from the experimental fatigue curves. Specifically, Eq. 5 overestimates fatigue strength and underestimates its reduction with the number of loading cycles.

The accuracy of the prediction here and below is quantitatively evaluated by a parameter κ characterizing the root mean square deviation of experimental and theoretical fatigue strengths:

$$\kappa = \sqrt{\frac{\sum_{i=1}^{l}\left(\sigma_{exp}(N_i) - \sigma_{theor}(N_i)\right)^2}{l}} \tag{6}$$

where σ_{exp} (N_i) designates the experimental maximum stress that caused failure at N_i cycles at the given stress

ratio, $\sigma_{\text{theor}}(N_i)$—predicted fatigue strength at N_i cycles, and l is the number of tests at the stress ratio considered. Equation 6 can be applied to characterize the spread of the experimental data with respect to the power-law approximation by means of parameter κ_0 defined as follows: $\kappa_0 = \sqrt{\frac{\sum_{i=1}^{l}\left(\sigma_{\exp}(N_i)-\sigma_{\text{appr}}(N_i)\right)^2}{l}}$ where $\sigma_{\text{appr}}(N_i) = (C - \log N_i)/B$ is evaluated using the regression relations with parameters presented in Table 1. A dimensionless parameter κ/κ_0 characterizes the relative accuracy of model prediction with respect to the approximation. The values of κ/κ_0 close to 1 indicate that the prediction is as close to the test data as the approximation, and larger κ/κ_0 reflects larger deviation between test results and theory. For κ and κ/κ_0 values corresponding to stress ratios at which prediction by the model was performed, see Table 2.

Strain energy density as a loading parameter

Strain energy density (SED) range has been considered as a parameter governing fatigue failure of fiber-reinforced polymer composites [23, 24] and incorporating the complex loading and stress ratio effects. At uniaxial loading, the range of SED is expressed as

$$\Delta W = \frac{1}{2}(\sigma_{\max}\varepsilon_{\max} - \sigma_{\min}\varepsilon_{\min}). \tag{7}$$

For linear elastic material, Eq. 7 can be recast in the form

$$\Delta W = \frac{1}{2E}(1 - R^2)\sigma_{\max}^2. \tag{8}$$

It follows form the relation Eq. 8 above that, at negligible reduction of the Young's modulus E during loading, SED range as a controlling parameter is equivalent to an effective stress defined by

$$\sigma_{\text{eff}} = \sqrt{1 - R^2}\sigma_{\max}. \tag{9}$$

The fatigue life should be a function of σ_{eff} only; hence, an experimental S–N curve at a fixed stress ratio provides sufficient information for establishing the functional form of $N = N(\sigma_{\text{eff}})$ and, based on it and Eq. 9, predicting fatigue life at an arbitrary stress ratio. Specifically, fatigue strength at a stress ratio R is related to that at R^* as follows:

$$\sigma_{f,R}(N) = \sqrt{\frac{1 - R^{*2}}{1 - R^2}}\sigma_{f,R^*}(N) \tag{10}$$

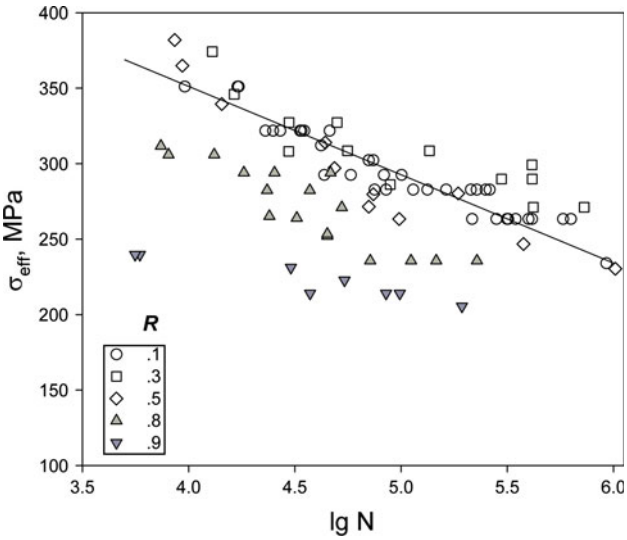

Fig. 3 Effective stress Eq. 9 versus number of load cycles to failure at several stress ratios

The accuracy of the SED range-based model can be evaluated by plotting the experimental fatigue data as a function of σ_{eff} and checking if they form a master curve. It is seen in Fig. 3 that for relatively low stress ratios, up to $R = 0.5$, the test data tend to collapse on a single curve (the line Fig. 3 corresponds to the effective stress Eq. 9 evaluated using the regression curve $\log N = C - B\sigma_{\max}$ of $R = 0.1$ test data with parameters given in Table 1). However, the S–N data at higher stress ratios, $R = 0.8$ and 0.9, deviate distinctly from this apparent master curve.

Further, we use Eq. 10 with $R^* = 0.1$ to predict fatigue strength for the other stress ratios considered, with the results plotted in Fig. 1b–e. The κ values shown in Table 2

Table 2 Discrepancy κ of model prediction and experimental fatigue strength data according to Eq. 6, in MPa (and relative discrepancy κ/κ_0)

Model	Stress ratio				
	$R = 0.1$	$R = 0.3$	$R = 0.5$	$R = 0.8$	$R = 0.9$
Static strength–fatigue life relation, Eq. 5	–	146 (2.5)	353 (5.8)	545 (4.6)	329 (8.9)
SED range-based effective stress, Eq. 10	–	86 (1.5)	68 (1.1)	366 (3.1)	633 (17)
Modified Goodman constant life diagram, Eq. 11	–	63 (1.1)	147 (2.4)	172 (1.4)	43 (1.2)
Constant life diagram, Eq. 12	–	99 (1.7)	262 (4.3)	284 (2.4)	68 (1.8)
Residual strength model, Eq. 16	–	99 (1.7)	110 (1.8)	442 (3.8)	416 (11.2)
Damage monitoring, Eq. 18	98 (1.7)	121 (2.1)	74 (1.2)	284 (2.4)	68 (1.8)

reveal a good agreement of Eq. 10 with test data only for the lower stress ratios of 0.3 and 0.5.

Constant fatigue life diagram

For construction of the constant life diagram in its simplest, linear form, experimental fatigue curve at one stress ratio and the static strengths are needed. In contrast to the classical linear Goodman diagram, shown schematically in Fig. 4a, for polymer–matrix composites the inflection point usually has to be shifted to $\eta \neq 0$ (the exact value depending on the mismatch of tensile and compressive strength [6, 31–33]). Moreover, the ultimate tensile strength should be replaced by the creep rupture strength at a time corresponding to the fatigue life [27], $t = N/f$ (where f is the frequency of loading), as shown in Fig. 4b.

For the present case of tension–tension fatigue, the fatigue strength at an arbitrary stress ratio $R > 0$, $\sigma_{f,R}(N)$, is easily derived from the linear Goodman diagram using experimental fatigue strength at stress ratio R^*, $\sigma_{f,R^*}(N)$, and creep strength at a time corresponding to the number of cycles N, $\sigma_{f,1}(N/f)$. The resulting expressions are

$$\sigma_{f,R}(N) = \frac{2\sigma_{f,1}(N/f)D}{(1+R)D+1-R} \tag{11}$$

$$D = \frac{\sigma_{f,R^*}(N)(1-R^*)}{2\sigma_{f,1}(N/f) - \sigma_{f,R^*}(N)(1+R^*)}$$

Having chosen $R^* = 0.1$, the S–N diagrams predicted by Eq. 11 for the rest of stress ratios studied are shown in Fig. 1b–e. A reasonably good agreement with the test results is observed. The effect of loading frequency on fatigue strength is close to negligible according to Eq. 11. Specifically, the difference in $\sigma_{f,R}$ evaluated by Eq. 11 is less than 1% for 2 and 17 Hz frequency within the durability range covered by tests at $R = 0.3$. The mentioned difference does not exceed 4% at $R = 0.9$. The theoretical S–N curves shown in Fig. 1 correspond to 4 Hz frequency of loading; the same predicted curves are also used in evaluation of discrepancy characteristic κ shown in Table 2.

A somewhat similar approach [34, 35] employs linear interpolation of fatigue strength as a function of stress ratio at a constant life

$$\sigma_{f,R}(N) = \sigma_{f,0}(N)(1-R) + \sigma_{f,1}(N/f)R. \tag{12}$$

If fatigue strength at $R = 0$ is not available, it can be evaluated using σ_{f,R^*} data at another stress ratio R^* in Eq. 12 as follows

$$\sigma_{f,0}(N) = \left(\sigma_{f,R^*}(N) - \sigma_{f,1}(N/f)R^*\right)/(1-R^*). \tag{13}$$

Choosing $R^* = 0.1$, the S–N diagrams predicted by Eqs. 12 and 13 at 4 Hz frequency of loading for the rest of stress ratios studied are shown in Fig. 1b–e. It is seen that the accuracy of prediction by Eq. 12 is somewhat inferior to that of Goodman diagram, Eq. 11, in that Eq. 12 provides consistently higher fatigue strength estimates (see also Table 2). The theoretical effect of loading frequency on fatigue strength according to Eq. 12 is limited and virtually coincides with that of Eq. 11.

Residual strength

Residual strength models take into account the stress ratio effect either by incorporating an ad hoc relation [36–39], usually with adjustable parameters, or by explicitly or implicitly distinguishing loading cycle- and time-dependent contributions to the strength reduction [2, 28, 29, 40].

The model of the stress ratio effect [2] is based on the integral relation for residual strength [41] modified by introducing separate contributions to strength reduction due to cyclic and static loads, with appropriate weights expressed in terms of R. At uniaxial tension–tension loading, the general expression, suitable for arbitrary loading program, reads as

$$\frac{\sigma_r}{\sigma_{\mathrm{st}}} = 1 - R\int_0^{t/t_{\mathrm{c}}} \left(1 - \frac{\sigma_{\max}}{\sigma_{\mathrm{st}}}\right) d\left(\frac{\tau}{t_{\mathrm{c}}}\right)^{j_{\mathrm{c}}} - (1-R)\int_0^{t/t_{\mathrm{f}}} \left(1 - \frac{\sigma_{\max}}{\sigma_{\mathrm{st}}}\right) d\left(\frac{\tau}{t_{\mathrm{f}}}\right)^{j_{\mathrm{f}}} \tag{14}$$

where t_{c} and t_{f} are the times to failure under constant $\sigma_{\max}$ for creep ($R = 1$) and fatigue ($R = 0$), and j_{c}, j_{f} are material parameters at static and cyclic fatigue, respectively. For constant-amplitude loading the integration of Eq. 14 is straightforward, leading to

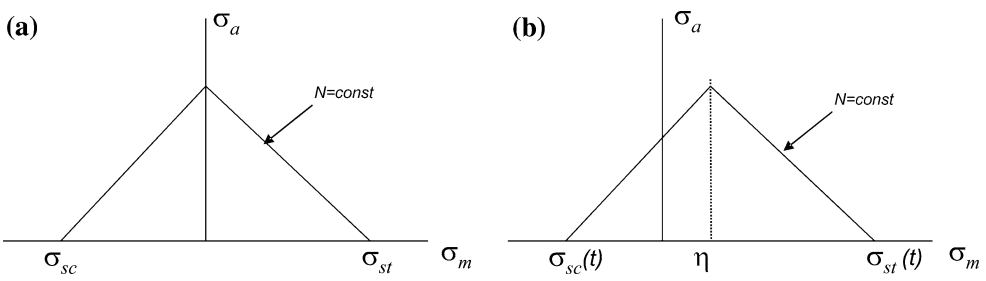

Fig. 4 Linear constant fatigue life diagrams: traditional (**a**) and accounting for the strength mismatch and time-dependence of strength (**b**)

$$\frac{\sigma_r}{\sigma_{st}} = 1 - R\left(1 - \frac{\sigma_{max}}{\sigma_{st}}\right)\left(\frac{t}{t_c}\right)^{j_c} - (1-R)\left(1 - \frac{\sigma_{max}}{\sigma_{st}}\right)\left(\frac{t}{t_f}\right)^{j_f}. \quad (15)$$

Enforcing the failure criterion $\sigma_r = \sigma_{max}$in Eq. 15 and simplifying the resulting expression, an implicit relation for fatigue lifetime t is finally obtained

$$R\left(\frac{t}{t_c}\right)^{j_c} + (1-R)\left(\frac{t}{t_f}\right)^{j_f} = 1 \quad (16)$$

The exponent j_c can be determined by fitting the time to failure under loading with a constant stress rate, predicted by Eq. 14 (at $R = 1$), to the respective test results [2, 42]. However, note that the value of $j_c = 1$ has been determined for different composites [2]. Furthermore, variation of the value of j_c is found to have a minor influence on the predicted static strength and lifetime under step-wise creep loading. Therefore, $j_c = 1$ is assumed in the following.

By derivation, j_f and t_f relate to cyclic loading at $R = 0$. The mentioned parameters are replaced by those relating to $R = 0.1$ loading for convenience [2], therefore in the following, as in [2], t_f is taken as lifetime under stress ratio of 0.1. Residual strength degradation under fatigue loading with $R = 0.1$ has been determined experimentally, and the estimate of $j_f = 1.33$ obtained [15].

Using the parameter values listed above, the experimental S–N curve at $R = 0.1$ and creep strength curve ($R = 1$), fatigue diagrams at 4 Hz frequency for the rest of stress ratios of loading were obtained by numerically solving Eq. 16 and plotted in Fig. 1b–e. It is seen that the agreement with test results is reasonable for the lower stress ratios, while the predicted fatigue strength is rather conservative for the higher stress ratios.

Damage monitoring

Monitoring the state of damage of a composite material during cyclic loading by, e.g., following stiffness reduction, hysteresis, autogenous heating temperature, etc., yields means for evaluation of the residual life provided the critical damage level is known. A fixed reduction of modulus has been found applicable as such a fatigue failure criterion for several glass fiber/polymer matrix composites [30, 43, 44].

It has been determined in a previous study [14] of the glass/polyester composite considered that the variation of strain amplitude ε_a, hence also compliance $A = \varepsilon_a/\sigma_a$, with the number of loading cycles n was close to linear for nearly all of the fatigue lifetime under constant σ_a loading. Thus the rate of compliance variation dA/dn did not change appreciably during lifetime of the composite. The relative increase of the compliance during loading, $c = (A - A_0)/A_0$, although exhibiting considerable scatter, did not depend on either stress ratio or maximum stress of the fatigue load [14]. These experimental findings enable evaluation of fatigue life of the composite material by measuring the rate of compliance variation dA/dn at the cyclic loading conditions of interest.

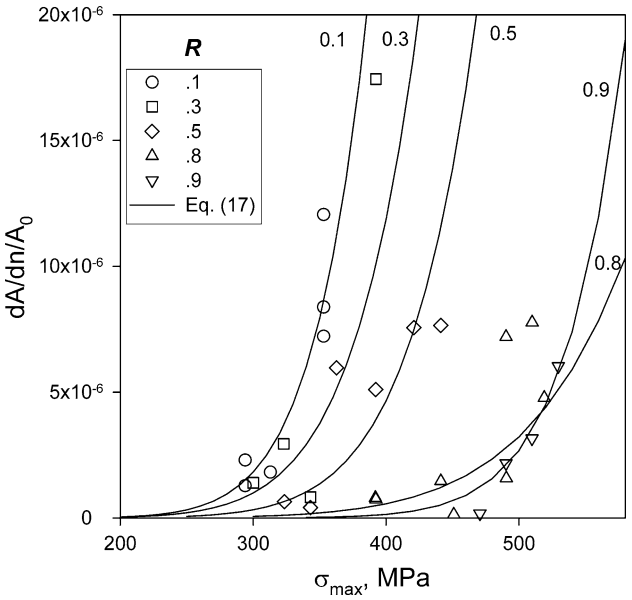

Fig. 5 The normalized rate of compliance as a function of maximum cycle stress at several stress ratios

The experimentally determined compliance rate is shown in Fig. 5 as a function of the maximum stress. The rate data are approximated by a power low relation

$$\frac{1}{A_0}\frac{dA}{dn} = a\sigma_{max}^{b} \quad (17)$$

for each stress ratio. Integrating Eq. 17, the relation for the S–N curve in terms of the normalized compliance rate parameters a, b and its limit variation during loading c (estimated [14] at 0.091) is obtained as follows

$$N = \frac{c}{a}\sigma_{max}^{-b}. \quad (18)$$

The fatigue life evaluated by Eq. 18 is in reasonably good agreement with the test results, as seen in Fig. 1.

Discussion

The fatigue models considered above for uniaxial cyclic loading with $R > 0$ employ differing amounts of experimental data to characterize the composite material. The mean and standard deviation of the static strength is sufficient for Kassapoglou's approach [18, 19]. An S–N curve at a fixed stress ratio has to be determined to apply the

strain energy density model [23, 24]. Apart from such a fatigue curve, creep strength data are also needed for implementing the linear constant fatigue life diagram as well as for Miyano's et al. [34, 35] fatigue model. In addition to that, an experimental characteristic of strength reduction during cyclic loading is employed in the residual strength-based fatigue model proposed by Guedes [2]. The variant of the damage monitoring-based life prediction [30, 43, 44] applied above entails experimental evaluation of damage accumulation rate as a function of cyclic stress level and the critical damage level at the stress ratios of interest.

The latter approach provides *S–N* diagrams Eq. 18 in good agreement with fatigue tests within the whole stress ratio range studied as seen in Fig. 1 and Table 2. However, the predictive capacity of the damage monitoring method is relatively low, because fatigue testing is needed at each stress ratio to evaluate damage rate and critical damage. Nevertheless, the approach can be used to assess high-cycle fatigue lifetime from short-duration cyclic tests as follows [45]: damage accumulation rate is measured in a short-term test at the low cyclic load level of interest, after which the load level is increased to accelerate damage accumulation, and decreased to the initial one shortly before failure to determine the critical damage level. Knowing the rate and the critical amount of damage, fatigue life the specimen would have at a constant-amplitude loading can be estimated. Thus both the damage accumulation rate and the critical damage level at the low stress are measured in a comparatively short-duration test allowing reduction of the total fatigue test duration by a factor of [45] 5–10. The lowest stress level for which such a method can be efficiently used is determined by the sensitivity of the material parameter monitored to damage.

The experimentally simpler models considered above, that use only one fatigue curve (strain energy density model, Fig. 3) or just static strength data (Kassapoglou's model, Fig. 1), appear applicable only within a rather narrow range of R as seen in Fig. 1 and Table 2.

As the reduction of dynamic modulus during loading was relatively small and did not depend appreciably on stress ratio [14], defining the effective stress based on Eq. 9 appears justified. It is also corroborated indirectly by the good agreement of prediction of Eq. 10 with the test results at the relatively small stress ratios, $R = 0.3$ and 0.5. Thus the discrepancy of energy density range-based model with test results at the higher stress ratios, $R = 0.8$ and 0.9, is likely to be caused by neglecting the effect of mean stress that becomes predominant at high R.

The performance of the static strength-based model is inconsistent in that in some cases the accuracy of prediction is remarkable while being poor for other composite materials or loading conditions [8, 18, 19]. It is claimed in

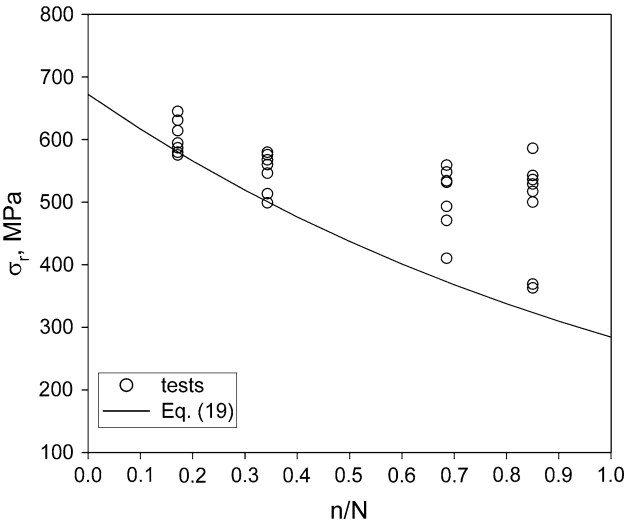

Fig. 6 Variation of residual strength as a function of the normalized duration of cyclic loading at $R = 0.1$ and $\sigma_{max} = 284$ MPa

[19] that the model [18] is associated with a specific residual strength relation

$$\sigma_r = \sigma_{\max}^{\frac{n}{N-1}} \sigma_{st}^{\frac{N-n-1}{N-1}}. \tag{19}$$

Thus the performance of Kassapoglou's model [18, 19] is likely to be related to the applicability of Eq. 19 for strength degradation of a given material. In the present case, Eq. 19 does not fit the experimental residual strength data [15] shown in Fig. 6 that is consistent with the unsatisfactory accuracy of fatigue prediction by Eq. 5 seen in Fig. 1.

Using a fatigue diagram at a low stress ratio ($R = 0.1$ here) and the creep strength diagram ($R = 1$) and interpolating the fatigue strength as either a linear function of mean cycle stress, Eq. 11, or stress ratio, Eq. 12, appears to provide an optimal trade-off between accuracy of prediction and amount of test data necessary. Applying a piecewise linear constant life diagram, as suggested in [8], would further increase the accuracy, but at the cost of cyclic testing at more than one stress ratio. Adding residual strength-derived information to fatigue and creep strength data, as in Guedes [2] Eq. 16, does not appear to increase the accuracy of fatigue life prediction. In fact, the theoretical estimate of fatigue strength becomes overly conservative at the higher stress ratios as seen in Fig. 1d and e.

Conclusions

Several empirical models capable of predicting the stress ratio effect on fatigue life have been applied to fatigue data of glass fiber/polyester matrix laminated composite in uniaxial tension–tension loading. The models varied in the amount of experimental data needed for their calibration.

The accuracy of prediction was generally found to improve with increasing the amount of test data used by a model. A linear constant life diagram, based on experimentally obtained fatigue data at a low stress ratio and creep strength data, provided reasonable trade-off between the accuracy of life prediction and the amount of test data necessary for implementation of the model.

References

1. Brinson LC, Gates TS (2000) In: Comprehensive composite materials, vol 2. Elsevier Science Ltd, New York, p 333
2. Guedes RM (2007) Compos Sci Technol 67:2574
3. Talreja R (2000) In: Comprehensive composite materials, vol 2. Elsevier Science Ltd, New York, p 529
4. Harris B, Gathercole N, Lee JA, Reiter H, Adam T (1997) Philos Trans R Soc Lond A 355:1259
5. Harris B, Carroll HE, Davies AJ (2003) Adv Compos Lett 12:7
6. Kawai M, Koizumi M (2007) Compos Part A 38:2342
7. Golub VP, Pogrebniak AD, Kochetkova ES (2008) Mech Compos Mater 44:65
8. Vassilopoulos AP, Manshadi BD, Keller T (2010) Int J Fatigue 32:659
9. Andersons J (1993) Mech Compos Mater 29:545
10. Degrieck J, Van Paepegem W (2001) Appl Mech Rev 54:279
11. Post NL, Case SW, Lesko JJ (2008) Int J Fatigue 30:2064
12. Passipoularidis VA, Philippidis TP (2009) Int J Fatigue 31:408
13. Quaresimin M, Susmel L, Talreja R (2010) Int J Fatigue 32:2
14. Tamužs V, Andersons J, Aniskevich K, Jansons J, Korsgaard J (1998) Mech Compos Mater 34:321
15. Andersons J, Korsgaard J (1999) Mech Compos Mater 35:395
16. Andersons J, Gruševckis I, Korsgaard J (1999) Mech Compos Mater 35:461
17. Andersons J, Korsgaard J (1997) The effect of stress ratio on durability and damage accumulation in GRP at uniaxial loading. In: Proceedings of international conference on fatigue composites, Paris, p 315
18. Kassapoglou C (2007) J Compos Mater 41:2737
19. Kassapoglou C (2010) J Compos Mater. doi:10.1177/0021998308104357
20. Conle A, Ingall JP (1985) J Compos Technol Res 7:3
21. Nasr M, Abouelwafa MN, Gomaa A, Hamdy A, Morsi E (2005) J Compos Mater 39:1283
22. Ellyin F, El Kadi H (1990) Compos Struct 15:61
23. El Kadi H, Ellyin F (1994) Composite 25:917
24. Petermann J, Plumtree A (2001) Compos Part A 32:107
25. Shokrieh MM, Taheri-Behrooz F (2006) Compos Struct 75:444
26. Sendeckyj GP (2001) Int J Fatigue 23:347
27. Owen MJ (1970) Composite 1:346
28. Epaarachchi JA (2006) Compos Struct 74:419
29. Loverich JS, Russell BE, Case SW, Reifsnider KL (2000) In: Schapery RA, Sun CT (eds) Time dependent and nonlinear effects in polymers and composites. ASTM STP 1357, p 310
30. Brøndsted P, Andersen SI, Lilholt H (1996) Mech Compos Mater 32:21
31. Oldyrev PP (1984) Mech Compos Mater 20:591
32. Rotem A, Nelson HG (1989) Compos Sci Technol 36:45
33. Limonov VA, Anderson YaA (1991) Mech Compos Mater 27:276
34. Miyano Y, Nakada M, Muki R (1999) Mech Time Depend Mater 3:141
35. Miyano Y, Nakada M, Kudoh H, Muki R (2000) J Compos Mater 34:538
36. Kim RY (1990) Effect of mean stresses on fatigue behavior of composite laminates. In: Proceedings of 7th international conference on composite materials, vol 2, p 621
37. Caprino G, Giorleo G (1999) Compos Part A 30:299
38. Caprino G (2000) J Compos Mater 34:1334
39. Epaarachchi JA, Clausen PD (2003) Compos Part A 34:313
40. Reifsnider K, Case S, Duthoit J (2000) Compos Sci Technol 60:2539
41. Reifsnider KL (1986) Eng Fract Mech 25:739
42. Guedes RM (2009) Compos Sci Technol 69:1200
43. Tamuzs V, Dzelzitis K, Reifsnider K (2004) Appl Compos Mater 11:281
44. Tamuzs V, Dzelzitis K, Reifsnider K (2008) Compos Sci Technol 68:2717
45. Oldirev PP, Parfeev VM, Komar VI (1977) Mech Polym 13:762